

Hopf bifurcation and oscillatory dynamics in a delayed FitzHugh-Nagumo neuronal network on scale-free topologies

Zhan Shen(申瞻), Qianqian Zheng(郑前前), Jianwei Yang(杨建伟), and Jianwei Shen(申建伟)
Citation: Chin. Phys. B, 2026, 35 (**6**): 060202. DOI: 10.1088/1674-1056/ae594c
http://cpb.iphy.ac.cn; http://iopscience.iop.org/cpb

What follows is a list of articles you may be interested in

Probabilistic distribution and stochastic *P*-bifurcation of a nonlinear energy-regenerative suspension system with time-delayed feedback control

Zhao-Bin Zeng(曾昭彬), Ya-Hui Sun(孙亚辉), and Yang Liu(刘洋)
Chin. Phys. B, 2026, 35 (**1**): 010201. DOI: 10.1088/1674-1056/ade669

Event-based nonfragile state estimation for memristive recurrent neural networks with stochastic cyber-attacks and sensor saturations

Xiao-Guang Shao(邵晓光), Jie Zhang(张捷), and Yan-Juan Lu(鲁延娟)
Chin. Phys. B, 2024, 33 (**7**): 070203. DOI: 10.1088/1674-1056/ad3dcb

Mechanism analysis of regulating Turing instability and Hopf bifurcation of malware propagation in mobile wireless sensor networks

Xi-Xi Huang(黄习习), Min Xiao(肖敏), Leszek Rutkowski, Hai-Bo Bao(包海波), Xia Huang(黄霞), and Jin-De Cao(曹进德)
Chin. Phys. B, 2024, 33 (**6**): 060202. DOI: 10.1088/1674-1056/ad24d5

Bifurcation and dynamics in double-delayed Chua circuits with periodic perturbation

Wenjie Yang(杨文杰)
Chin. Phys. B, 2022, 31 (**2**): 020201. DOI: 10.1088/1674-1056/ac1e0b

Coexisting hidden attractors in a 4D segmented disc dynamo with one stable equilibrium or a line equilibrium

Jianghong Bao(鲍江宏), Dandan Chen(陈丹丹)
Chin. Phys. B, 2017, 26 (**8**): 080201. DOI: 10.1088/1674-1056/26/8/080201

SPECIAL TOPIC — Biophysical circuits: Modeling & applications in neuroscience

Hopf bifurcation and oscillatory dynamics in a delayed FitzHugh–Nagumo neuronal network on scale-free topologies

Zhan Shen(申瞻)[1,2], Qianqian Zheng(郑前前)[2,†], Jianwei Yang(杨建伟)[1], and Jianwei Shen(申建伟)[1,‡]

[1] *School of Mathematics and Statistics, North China University of Water Resources and Electric Power, Zhengzhou* 450046, *China*
[2] *School of Science, Xuchang University, Xuchang* 461000, *China*

(Received 4 February 2026; revised manuscript received 27 March 2026; accepted manuscript online 31 March 2026)

Neuronal oscillations arise from the interplay between intrinsic neuronal dynamics and network connectivity. In this work, we investigate the effects of network topology on oscillatory behavior in a FitzHugh–Nagumo (FHN) neuronal model with distributed delay, representing ion-channel memory effects, and diffusive delay, accounting for axonal transmission delays. The neurons are coupled through quasi-Laplacian interactions on Barabási–Albert (BA) scale-free networks. Using the multiple-time-scales (MTS) method, we derive amplitude equations near the Hopf bifurcation point and establish explicit relationships between oscillatory dynamics and network topology. The analysis shows that the smallest negative eigenvalue of the network governs the critical delay threshold for oscillation onset, while the distributed-delay parameter σ and diffusive delay τ jointly regulate this threshold. The resulting oscillation frequencies are confined to the beta band (15–30 Hz), a frequency range often associated with pathological neural activity in Parkinson's disease. Extensive numerical simulations over 50 network realizations confirm the theoretical predictions. Hub nodes with higher degrees exhibit lower critical delays and larger oscillation amplitudes, whereas peripheral nodes display weaker and more heterogeneous responses. Statistical analysis further reveals a negative correlation between node degree and critical delay and a positive correlation between node degree and oscillation amplitude. These results demonstrate how delay effects and network topology jointly shape the emergence and spatial organization of collective oscillations, providing insights into synchronization phenomena in complex neuronal networks.

Keywords: Hopf bifurcation, FitzHugh–Nagumo (FHN) model, delay, multiple-time-scales (MTS) method, quasi-Laplacian, Barabási–Albert (BA) scale-free network

PACS: 02.30.Ks, 02.30.Oz, 02.30.–f

DOI: 10.1088/1674-1056/ae594c **CSTR:** 32038.14.CPB.ae594c

1. Introduction

The Hodgkin–Huxley (HH) model, first proposed by Hodgkin and Huxley in 1952, laid the foundation for research in neuronal dynamics.[1] The FitzHugh–Nagumo (FHN) model is a simplified reduction of the HH model, involving only two dynamical variables: the membrane potential and a recovery variable.[2] Owing to its simplicity and its ability to reproduce the essential mechanism of neuronal firing, the FHN model has been widely adopted in theoretical studies of neuronal excitability and oscillatory dynamics. The brain consists of billions of neurons interconnected via synapses,[3] forming large-scale networks with highly heterogeneous connectivity. Consequently, complex network theory has become an indispensable framework for describing neuronal interactions beyond isolated or locally coupled systems. Among various network models, the Barabási–Albert (BA) scale-free network was introduced to explain the emergence of power-law degree distributions observed in many real-world systems.[4] Owing to its preferential attachment mechanism, the BA network is characterized by a few highly connected hub nodes and a large number of low-degree peripheral nodes, resulting in strong structural heterogeneity. Rather than serving as an exact representation of anatomical brain networks, scale-free networks provide a minimal and mechanism-oriented platform for investigating how degree heterogeneity influences collective neuronal dynamics. Empirical and theoretical studies have revealed functional distinctions between hub nodes and peripheral nodes in heterogeneous networks. For instance, Tanaka *et al.*[5] showed that dynamical robustness is mainly determined by peripheral nodes, whereas structural robustness relies on hub nodes. Moon *et al.*[6] established general mathematical relations linking global topology (node degree), local dynamics (oscillation amplitude), and directional information flow (phase lead/lag), thereby revealing a fundamental rule governing information transmission in brain networks. More recently, Kocsis *et al.*[7] highlighted the critical role of hub nodes in semantic processing within the human brain. From a dynamical systems perspective, it has been shown that, in heterogeneous networks, the onset of collective instabilities is often controlled by spectral properties associated with

[†]Corresponding author. E-mail: zqq@xcu.edu.cn
[‡]Corresponding author. E-mail: xcjwshen@gmail.com

© 2026 Chinese Physical Society and IOP Publishing Ltd. All rights, including for text and data mining, AI training, and similar technologies, are reserved.

highly connected nodes, leading to earlier destabilization of hub-related modes.[8,9] In this paper, we conduct an in-depth investigation of the relationship among node degree, time delay, and oscillation amplitude in BA networks. Extensive numerical experiments are performed, and the corresponding statistical results are presented.

Pattern formation is ubiquitous in nature, ranging from animal coat markings to synchronous neuronal discharges, reflecting the emergence of spatiotemporal coherence and self-organization. In 1952, Turing[10] introduced a pioneering theory of morphogenesis based on reaction–diffusion systems, explaining the mechanism of spontaneous pattern formation. In his work, Turing demonstrated that a homogeneous equilibrium in an activator–inhibitor system can be destabilized through diffusion-driven instability, leading to nonuniform steady states. Turing instability has since provided a universal framework for understanding pattern formation across natural and artificial systems. In 2010, Nakao and Mikhailov[11] established a theoretical framework for Turing instability on complex networks, laying the foundation for studying pattern dynamics in network systems. This seminal work showed that network eigenvalues serve as effective control parameters for pattern-forming bifurcations. Subsequently, Asllani *et al.*[12] extended this framework from undirected to directed networks, emphasizing that both network topology and local dynamical rules play equally essential roles. This extension has opened new perspectives for modeling dynamical systems in neuroscience. Zheng *et al.*[13] further combined reaction–diffusion equations with complex networks and showed that positive wave numbers can induce Turing patterns.

Clinical neurophysiological studies have demonstrated that pathological beta-band (15–30 Hz) synchronous oscillations are prevalent within the basal ganglia–cortical loops of patients with Parkinson's disease, serving as a primary dynamical hallmark of motor impairment.[14–16] From the perspective of nonlinear dynamics, Hopf bifurcation represents the fundamental mechanism by which a system transitions from a steady state to limit-cycle oscillations. This provides a crucial theoretical framework and a novel avenue for elucidating how neuronal populations transition from stochastic firing to pathological rhythmic activity.

While Turing instability gives rise to stationary spatial patterns, neuronal oscillations are typically associated with Hopf bifurcations, which generate time-periodic activity. In networked systems, Hopf bifurcation is likewise shaped by the spectral properties of the coupling operator, a principle closely related to the master stability framework.[17] Time delay is an intrinsic feature of neuronal systems, arising from finite axonal conduction velocities and synaptic transmission delays.[18] Delay is well known to induce instabilities, bifurcations, and pattern formation.[19–22] Furthermore, the kinetics of ion channels are not governed solely by fixed delays but also exhibit memory effects, whereby the present state depends on the weighted history of past states with exponential decay. To capture this feature, distributed delay kernels have been introduced into neuronal models. Karmeshu *et al.*[23] incorporated a distributed delay kernel into a single-neuron firing model, enabling the system to account for the weighted influence of past membrane potentials. Experiments have shown that postsynaptic currents (PSCs), driven by neurotransmitter–receptor interactions, typically decay exponentially rather than vanish instantaneously.[24] Tiganj *et al.*[25] developed a single-neuron model based on calcium dynamics and calcium-activated nonspecific (CAN) cationic currents, demonstrating that individual neurons can generate firing activity with long exponential decay constants. These findings provide strong biological justification for incorporating distributed delay kernels into neuronal models. From a dynamical viewpoint, distributed delays act as temporal filters that modulate instability thresholds and oscillation amplitudes without altering the fundamental bifurcation structure.[26,27] Moreover, since neuronal signal transmission along axons also exhibits delays, introducing time delay into the diffusion term yields a more realistic description of neural signaling. The stability of delayed neuronal networks has been extensively investigated, revealing that delays can reorganize collective oscillatory behavior.[28,29] In addition, extensive studies have been devoted to the mathematical treatment of distributed delays in dynamical systems.[30,31] The derivation of amplitude equations for Hopf bifurcations in models with distributed delay is often based on the center manifold theorem.[32,33] This paper, for the first time, employs the multiple-time-scales method to derive the amplitude equation of Hopf bifurcation for a system incorporating both distributed delay and fixed delay in the diffusion term.

This study first focuses on the roles of distributed delay, representing ionic channel memory effects, and diffusive delay, associated with axonal signal transmission, in shaping the generation and regulation of neuronal oscillations. Building on this, we employ the multiple-time-scales (MTS) method to derive the amplitude equation and establish its explicit connection to the BA scale-free network topology, thereby linking node degree to local dynamical behavior. Our analysis reveals that the critical delay for oscillation onset is governed by the smallest negative eigenvalue of the network, while degree heterogeneity leads to effective coupling amplification at hub nodes. As a consequence, hub nodes undergo Hopf bifurcation at shorter delay thresholds and exhibit larger oscillation amplitudes than peripheral nodes. Extensive numerical simulations and statistical analyses across multiple network realizations confirm these theoretical predictions. The results provide a mechanistic explanation for the privileged role of hub nodes in delay-induced neuronal oscillations and highlight how struc-

tural heterogeneity biases collective dynamics. The structure of this paper is as follows. In Section 2, we introduce the proposed model and conduct stability analysis. In Section 3, we apply the multiple-time-scales method to derive the amplitude equation of Hopf bifurcation with both distributed delay and diffusive delay. Section 4 presents numerical simulations and discusses the biological implications. Finally, concluding remarks are provided.

2. The description of FHN model with delay and network

The general FHN model, incorporating distributed delay, time delay, and network structure, is given by

$$\begin{cases} \dfrac{\mathrm{d}u_i}{\mathrm{d}t} = -bu_i(u_i-a)(u_i-1) - \int_{-\infty}^{t} F(t-s)v_i(s)\,\mathrm{d}s \\ \qquad\qquad + d_1 \sum\limits_{j=1}^{N} Q_{ij}(u_j(t-\tau)-u_0), \\ \dfrac{\mathrm{d}v_i}{\mathrm{d}t} = \varepsilon(u_i + c - \beta v_i) + d_2 \sum\limits_{j=1}^{N} Q_{ij}(v_j(t-\tau)-v_0), \end{cases} \tag{1}$$

where u_i and v_i represent the membrane potential and recovery variable of the i-th neuron, respectively. The recovery variable v_i governs the slower dynamics associated with the activation of outward K^+ channel currents and the inactivation of inward Na^+ channel currents, while d_1 and d_2 denote the synaptic coupling strength and ionic diffusion coupling strength, respectively. The term $Q_{ij} = A_{ij} - \mu k_i \delta_{ij}$, with $\mu \in [0,1]$, describes the interactions among neurons in the network, where A is the adjacency matrix of an undirected and unweighted network, $k_i = \sum_{j=1}^{N} A_{ij}$ is the degree of node i, and δ_{ij} is the Kronecker delta. Notably, Q_{ij} reduces to the negative Laplacian matrix L_{ij} when $\mu = 1$, corresponding to a conservative zero-flux boundary condition that is biologically reasonable for neural network studies. The coupling term in the first equation of Eq. (1) physically represents the total synaptic current received by the target neuron i from its connected neighboring neurons in the network. The discrete time delay τ denotes the synaptic and axonal conduction delays, as the propagation of action potentials along axons and the release of neurotransmitters across synaptic clefts in biological systems require finite, nonzero time. The coupling term in the second equation represents the diffusion dynamics of K^+ and Na^+ ions between adjacent neurons, with τ denoting the delay associated with ion diffusion through ion channels. The distributed delay term $\int_{-\infty}^{t} F(t-s)v_i(s)\,\mathrm{d}s$ represents the memory effect arising from K^+ and Na^+ ion-channel kinetics. The weak kernel $F(x)$ and its corresponding integral term characterize the fact that the current state of a neuron is not determined solely by its instantaneous input, but is also influenced by the cumulative effect of the historical states of the recovery variable over a preceding time interval.

We consider the weak kernel

$$F(x) = \sigma \mathrm{e}^{-\sigma x}, \tag{2}$$

where $\sigma > 0$, and $1/\sigma$ reflects the mean delay of the weak kernel. Let $w_i(t) = \int_{-\infty}^{t} F(t-s)v_i(s)\,\mathrm{d}s$; then, we have

$$\begin{cases} \dfrac{\mathrm{d}u_i}{\mathrm{d}t} = -bu_i(u_i-a)(u_i-1) - w_i \\ \qquad\qquad + d_1 \sum\limits_{j=1}^{N} Q_{ij}(u_j(t-\tau)-u_0), \\ \dfrac{\mathrm{d}v_i}{\mathrm{d}t} = \varepsilon(u_i + c - \beta v_i) \\ \qquad\qquad + d_2 \sum\limits_{j=1}^{N} Q_{ij}(v_j(t-\tau)-v_0), \\ \dfrac{\mathrm{d}w_i}{\mathrm{d}t} = -\sigma w_i + \sigma v_i. \end{cases} \tag{3}$$

The positive equilibrium of system (3) is denoted by (u_0, v_0, w_0). Let $\Delta u_i = u_i - u_0$, $\Delta v_i = v_i - v_0$, and $\Delta w_i = w_i - w_0$ represent small perturbations. The linearized system of Eq. (3) around (u_0, v_0, w_0) can be written as follows:

$$\begin{bmatrix} \Delta \dot{u}_i \\ \Delta \dot{v}_i \\ \Delta \dot{w}_i \end{bmatrix} = \boldsymbol{J} \begin{bmatrix} \Delta u_i \\ \Delta v_i \\ \Delta w_i \end{bmatrix} + \boldsymbol{D} \begin{bmatrix} \sum_{j=1}^{N} Q_{ij} \Delta u_{j\tau} \\ \sum_{j=1}^{N} Q_{ij} \Delta v_{j\tau} \\ 0 \end{bmatrix}, \tag{4}$$

where

$$\boldsymbol{J} = \begin{bmatrix} -3bu_0^2 + 2(b+ab)u_0 - ab & 0 & -1 \\ \varepsilon & -\varepsilon\beta & 0 \\ 0 & \sigma & -\sigma \end{bmatrix},$$

$$\boldsymbol{D} = \begin{bmatrix} d_1 & 0 & 0 \\ 0 & d_2 & 0 \\ 0 & 0 & 0 \end{bmatrix},$$

and $u_i = u_i(t)$, $v_i = v_i(t)$, $u_{i\tau} = u_{i\tau}(t-\tau)$, and $v_{i\tau} = v_{i\tau}(t-\tau)$.

Let $\Lambda_N \le \cdots \le 0 \le \cdots \Lambda_1$ be the eigenvalues and $\phi^{(\alpha)} = (\phi_1^{(\alpha)}, \phi_2^{(\alpha)}, \ldots, \phi_N^{(\alpha)})$ be the eigenvectors of the quasi-Laplacian matrix Q_{ij}, satisfying $\sum_{j=1}^{N} Q_{ij}\phi_j^{(\alpha)} = \Lambda_\alpha \phi_i^{(\alpha)}$, $\forall \alpha = 1, 2, \ldots, N$. The general solution of system (4) is given by

$$\begin{cases} \Delta u_i = \sum\limits_{\alpha=1}^{N} \xi_1 \mathrm{e}^{\lambda_\alpha t} \phi_i^{(\alpha)}, \\ \Delta v_i = \sum\limits_{\alpha=1}^{N} \xi_2 \mathrm{e}^{\lambda_\alpha t} \phi_i^{(\alpha)}, \\ \Delta w_i = \sum\limits_{\alpha=1}^{N} \xi_3 \mathrm{e}^{\lambda_\alpha t} \phi_i^{(\alpha)}. \end{cases} \tag{5}$$

Substituting Eq. (5) into Eq. (4), we obtain

$$\lambda_\alpha \begin{bmatrix} \xi_1 \\ \xi_2 \\ \xi_3 \end{bmatrix} = \begin{bmatrix} a_{11} & a_{12} & a_{13} \\ a_{21} & a_{22} & a_{23} \\ a_{31} & a_{32} & a_{33} \end{bmatrix} \begin{bmatrix} \xi_1 \\ \xi_2 \\ \xi_3 \end{bmatrix}, \tag{6}$$

where

$$a_{11} = -3bu_0^2 + 2(b+ab)u_0 - ab + d_1 \Lambda_\alpha \mathrm{e}^{-\lambda_\alpha \tau},$$

$$
\begin{aligned}
a_{12} &= 0,\ a_{13} = -1,\\
a_{21} &= \varepsilon,\ a_{22} = -\varepsilon\beta + d_2\Lambda_\alpha \mathrm{e}^{-\lambda_\alpha\tau},\ a_{23} = 0,\\
a_{31} &= 0,\ a_{32} = \sigma,\ a_{33} = -\sigma.
\end{aligned}
$$

According to system (6), the corresponding characteristic equation of system (3) is

$$
\begin{aligned}
&\lambda_\alpha^3 + \left(m_1 + m_2\mathrm{e}^{-\lambda_\alpha\tau}\right)\lambda_\alpha^2\\
&+\left(m_3 + m_4\mathrm{e}^{-\lambda_\alpha\tau} + m_5\mathrm{e}^{-2\lambda_\alpha\tau}\right)\lambda_\alpha\\
&+m_6 + m_7\mathrm{e}^{-\lambda_\alpha\tau} + m_8\mathrm{e}^{-2\lambda_\alpha\tau} = 0. \qquad (7)
\end{aligned}
$$

The coefficients in Eq. (7) are given in Appendix A(a).

2.1. The stability without network

According to Eq. (7), the characteristic equation of system (3) in the absence of network coupling is

$$\lambda_\alpha^3 + m_1\lambda_\alpha^2 + m_3\lambda_\alpha + m_6 = 0. \qquad (8)$$

Theorem 1

Based on Eq. (8):

(i) If $H_{11}: m_1 > 0$, $H_{12}: m_3 > 0$, $H_{13}: m_6 > 0$, and $H_{14}: m_1m_3 - m_6 > 0$ hold, then system (3) is stable;

(ii) Otherwise, system (3) is unstable.

2.2. The stability without time delay

According to Eq. (7), the characteristic equation of system (3) in the absence of time delay is

$$
\begin{aligned}
&\lambda_\alpha^3 + (m_1+m_2)\lambda_\alpha^2 + (m_3+m_4+m_5)\lambda_\alpha\\
&+m_6 + m_7 + m_8 = 0. \qquad (9)
\end{aligned}
$$

Theorem 2

Based on Theorem 1(i) and Eq. (9),

(i) If Λ_α satisfies $H_{21}: m_1+m_2 > 0$, $H_{22}: m_3+m_4+m_5 > 0$, $H_{23}: m_6+m_7+m_8 > 0$, and $H_{24}: (m_1+m_2)(m_3+m_4+m_5) - (m_6+m_7+m_8) > 0$, then a Hopf bifurcation cannot occur in system (3).

(ii) Otherwise, Hopf bifurcation may occur in system (3).

2.3. The stability with network and time delay

Let $\lambda_\alpha = \mathrm{i}\omega_\alpha$ ($\omega_\alpha > 0$) be a solution of Eq. (7). Applying Euler's formula ($\mathrm{e}^{\mathrm{i}\theta} = \cos\theta + \mathrm{i}\sin\theta$) and separating the real and imaginary parts, we obtain

$$\cos(\theta) = \frac{A_1B_3 - A_3B_2}{A_1B_1 - A_2B_2},\quad \sin(\theta) = \frac{A_3B_1 - A_2B_3}{A_1B_1 - A_2B_2}, \qquad (10)$$

where $\theta = \omega_\alpha\tau$, and the expressions for A_1, A_2, A_3, B_1, B_2, and B_3 are given in Appendix A(b).

Furthermore, we obtain

$$\omega_\alpha^{12} + C_5\omega_\alpha^{10} + C_4\omega_\alpha^8 + C_3\omega_\alpha^6 + C_2\omega_\alpha^4 + C_1\omega_\alpha^2 + C_0 = 0, \qquad (11)$$

where the explicit expressions for C_0, C_1, C_2, C_3, C_4, and C_5 are given in Appendix A(c).

Let Eq. (11) be denoted by

$$
\begin{aligned}
g(\omega_\alpha) &= \omega_\alpha^{12} + C_5\omega_\alpha^{10} + C_4\omega_\alpha^8 + C_3\omega_\alpha^6\\
&\quad + C_2\omega_\alpha^4 + C_1\omega_\alpha^2 + C_0. \qquad (12)
\end{aligned}
$$

It follows that $\lim\limits_{\omega_\alpha\to\infty} g(\omega_\alpha) = +\infty$. Therefore, if $C_0 < 0$, Eq. (11) possesses at least one positive root. Without loss of generality, we assume that Eq. (11) has twelve positive roots, denoted by $\omega_{\alpha i}$ ($i = 1, 2, \ldots, 12$). Thus,

$$
\begin{aligned}
\tau_\alpha^k &= \frac{1}{\omega_{\alpha i}}\arccos\left(\frac{A_1B_3 - A_3B_2}{A_1B_1 - A_2B_2}\right) + \frac{2k\pi}{\omega_{\alpha i}},\\
k &= 0, 1, \ldots,
\end{aligned}
$$

and the critical delay value is defined as

$$\tau_* = \min\{\tau_\alpha^k\}. \qquad (13)$$

The transversality condition can be expressed as

$$
\begin{aligned}
\mathrm{Re}\left\{\left(\frac{\mathrm{d}\lambda_\alpha}{\mathrm{d}\tau}\right)^{-1}\right\}\Big|_{\tau=\tau_\alpha^k} &= \mathrm{Re}\left\{\frac{D_1 + D_2\mathrm{i}}{D_3 + D_4\mathrm{i}}\right\}\\
&= \frac{D_1D_3 + D_2D_4}{D_3^2 + D_4^2}, \qquad (14)
\end{aligned}
$$

where the expressions of D_1, D_2, D_3, and D_4 are given in Appendix A(d).

Theorem 3

Based on Theorem 2(i), Eqs. (13) and (14)

(i) If

$$D_3^2 + D_4^2 \neq 0,\ \ \mathrm{Re}\left\{\left(\frac{\mathrm{d}\lambda_\alpha}{\mathrm{d}\tau}\right)^{-1}\right\}\Big|_{\tau=\tau_\alpha^k} = 0,$$

then Hopf bifurcation cannot occur in system (3);

(ii) If

$$D_3^2 + D_4^2 \neq 0,\ \ \mathrm{Re}\left\{\left(\frac{\mathrm{d}\lambda_\alpha}{\mathrm{d}\tau}\right)^{-1}\right\}\Big|_{\tau=\tau_\alpha^k} \neq 0,$$

then the transversality condition holds:

(*) if $\tau < \tau_*$, system (3) is stable;

(**) if $\tau > \tau_*$, Hopf bifurcation occurs.

3. Amplitude equations for the Hopf bifurcaton

In this section, we derive the amplitude equation and determine the direction of the Hopf bifurcation using the method of MTS. By applying the transformation $(\Delta u_i, \Delta v_i, \Delta w_i)^{\mathrm{T}} = (u_i - u_0, v_i - v_0, w_i - w_0)^{\mathrm{T}}$ and treating $(\Delta u_i, \Delta v_i, \Delta w_i)^{\mathrm{T}}$ as $(u_i, v_i, w_i)^{\mathrm{T}}$, and defining $\tau_0^0 := \tau_*$ and $\omega_0 := \omega_*$, with the rescaling $t \to t\tau$, system (3) can be rewritten as

$$\dot{\boldsymbol{X}}_i = \tau\boldsymbol{G}_t\boldsymbol{X}_i + \tau\boldsymbol{G}_\tau\boldsymbol{X}_{i\tau} + \tau\boldsymbol{N}(\boldsymbol{X}_i), \qquad (15)$$

where

$$\boldsymbol{X}_i = \big(u_i(t),\ v_i(t),\ w_i(t)\big)^{\mathrm{T}},$$

$$\boldsymbol{X}_{i\tau} = \big(u_{i\tau}(t-1),\ v_{i\tau}(t-1),\ w_{i\tau}(t-1)\big)^{\mathrm{T}},$$

$$\boldsymbol{G}_t = \begin{bmatrix} b*11 & b_{12} & b_{13} \\ b_{21} & b_{22} & b_{23} \\ b_{31} & b_{32} & b_{33} \end{bmatrix},$$

$$\boldsymbol{G}_\tau = \begin{bmatrix} c*11 & c_{12} & c_{13} \\ c_{21} & c_{22} & c_{23} \\ c_{31} & c_{32} & c_{33} \end{bmatrix},$$

$$b_{11} = -3bu_0^2 + 2(b+ab)u_0 - ab,\ \ b_{12} = 0,\ \ b_{13} = -1,$$

$$b_{21} = \varepsilon,\ \ b_{22} = -\varepsilon\beta,\ \ b_{23} = 0,\ \ b_{31} = 0,$$

$$b_{32} = \sigma,\ \ b_{33} = -\sigma,$$

$$c_{11} = d_1 \sum_{j=1}^{N} L_{ij} + d_1 k_i (1-\mu),$$

$$c_{22} = d_2 \sum_{j=1}^{N} L_{ij} + d_2 k_i (1-\mu),$$

$$c_{12} = c_{13} = c_{21} = c_{23} = c_{31} = c_{32} = c_{33} = 0,$$

$$\boldsymbol{N}(\boldsymbol{X}_i) = \begin{bmatrix} \sum\limits_{|\alpha|=2}^{3} \frac{1}{\alpha!} D^\alpha f(\boldsymbol{X}_i) \cdot \boldsymbol{X}_i^\alpha \\ \sum\limits_{|\alpha|=2}^{3} \frac{1}{\alpha!} D^\alpha g(\boldsymbol{X}_i) \cdot \boldsymbol{X}_i^\alpha \\ \sum\limits_{|\alpha|=2}^{3} \frac{1}{\alpha!} D^\alpha h(\boldsymbol{X}_i) \cdot \boldsymbol{X}_i^\alpha \end{bmatrix} + O(4),$$

where $f_{u_iu_i} = (-3u_0+1+a)b$, $f_{u_iu_iu_i} = -6b$, and all other terms vanish. Therefore,

$$\boldsymbol{N}(\boldsymbol{X}_i) = \begin{bmatrix} (-3u_0+1+a)bu_i^2 - bu_i^3 + O(4) & 0 & 0 \end{bmatrix}.$$

Define the time scales as $T_0 = t$ and $T_2 = \varepsilon^2 t$. Then,

$$\frac{\partial}{\partial t} = \frac{\partial}{\partial T_0} + \varepsilon^2 \frac{\partial}{\partial T_2}, \tag{16}$$

where ε is a small perturbation parameter.

The solution $\boldsymbol{X}_i$ can be expanded as

$$\begin{aligned} \boldsymbol{X}_i(T_0,T_2) &= \begin{bmatrix} u_i(T_0,T_2) \\ v_i(T_0,T_2) \\ w_i(T_0,T_2) \end{bmatrix} \\ &= \varepsilon \begin{bmatrix} u_i^{(1)}(T_0,T_2) \\ v_i^{(1)}(T_0,T_2) \\ w_i^{(1)}(T_0,T_2) \end{bmatrix} + \varepsilon^2 \begin{bmatrix} u_i^{(2)}(T_0,T_2) \\ v_i^{(2)}(T_0,T_2) \\ w_i^{(2)}(T_0,T_2) \end{bmatrix} \\ &\quad + \varepsilon^3 \begin{bmatrix} u_i^{(3)}(T_0,T_2) \\ v_i^{(3)}(T_0,T_2) \\ w_i^{(3)}(T_0,T_2) \end{bmatrix} + O(4). \end{aligned} \tag{17}$$

From Eq. (17), we obtain

$$\begin{aligned} \boldsymbol{X}_{i\tau}(T_0-1,T_2) &= \begin{bmatrix} u_{i\tau}(T_0-1,T_2) \\ v_{i\tau}(T_0-1,T_2) \\ w_{i\tau}(T_0-1,T_2) \end{bmatrix} \\ &= \sum_{j=1}^{3} \varepsilon^j \begin{bmatrix} u_{i\tau}^{(j)}(T_0-1,T_2) \\ v_{i\tau}^{(j)}(T_0-1,T_2) \\ w_{i\tau}^{(j)}(T_0-1,T_2) \end{bmatrix} - \varepsilon^3 \frac{\partial}{\partial T_2} \begin{bmatrix} u_{i\tau}^{(1)}(T_0-1,T_2) \\ v_{i\tau}^{(1)}(T_0-1,T_2) \\ w_{i\tau}^{(1)}(T_0-1,T_2) \end{bmatrix} \\ &\quad + \cdots. \end{aligned} \tag{18}$$

The nonlinear term can be expanded as

$$\boldsymbol{N} = \varepsilon^2 \boldsymbol{N}^{(2)} + \varepsilon^3 \boldsymbol{N}^{(3)} + O(4). \tag{19}$$

where

$$\boldsymbol{N}^{(2)} = \begin{bmatrix} (-3u_0+1+a)b\big(u_i^{(1)}\big)^2 \\ 0 \\ 0 \end{bmatrix},$$

$$\boldsymbol{N}^{(3)} = \begin{bmatrix} -b\big(u_i^{(1)}\big)^3 \\ 0 \\ 0 \end{bmatrix}.$$

A small perturbation is introduced to the parameter τ, namely, $\tau = \tau_* + \varepsilon^2\delta$, where $\delta > 0$. In addition, let $\boldsymbol{G}_t|_{\tau=\tau_*} = \boldsymbol{G}_t^*$ and $\boldsymbol{G}_\tau|_{\tau=\tau_*} = \boldsymbol{G}_\tau^*$. Substituting Eqs. (16)–(19) into Eq. (15), we obtain

$O(\varepsilon)$:

$$\frac{\partial}{\partial T_0} \begin{bmatrix} u_i^{(1)} \\ v_i^{(1)} \\ w_i^{(1)} \end{bmatrix} - \tau_* \boldsymbol{G}_t^* \begin{bmatrix} u_i^{(1)} \\ v_i^{(1)} \\ w_i^{(1)} \end{bmatrix} - \tau_* \boldsymbol{G}_\tau^* \begin{bmatrix} u_{i\tau}^{(1)} \\ v_{i\tau}^{(1)} \\ w_{i\tau}^{(1)} \end{bmatrix} = 0. \tag{20}$$

$O(\varepsilon^2)$:

$$\frac{\partial}{\partial T_0} \begin{bmatrix} u_i^{(2)} \\ v_i^{(2)} \\ w_i^{(2)} \end{bmatrix} - \tau_* \boldsymbol{G}_t^* \begin{bmatrix} u_i^{(2)} \\ v_i^{(2)} \\ w_i^{(2)} \end{bmatrix} - \tau_* \boldsymbol{G}_\tau^* \begin{bmatrix} u_{i\tau}^{(2)} \\ v_{i\tau}^{(2)} \\ w_{i\tau}^{(2)} \end{bmatrix} = \tau_* \boldsymbol{N}^{(2)}. \tag{21}$$

$O(\varepsilon^3)$:

$$\begin{aligned} &\frac{\partial}{\partial T_0} \begin{bmatrix} u_i^{(3)} \\ v_i^{(3)} \\ w_i^{(3)} \end{bmatrix} - \tau_* \boldsymbol{G}_t^* \begin{bmatrix} u_i^{(3)} \\ v_i^{(3)} \\ w_i^{(3)} \end{bmatrix} - \tau_* \boldsymbol{G}_\tau^* \begin{bmatrix} u_{i\tau}^{(3)} \\ v_{i\tau}^{(3)} \\ w_{i\tau}^{(3)} \end{bmatrix} \\ &= -\frac{\partial}{\partial T_2} \begin{bmatrix} u_i^{(1)} \\ v_i^{(1)} \\ w_i^{(1)} \end{bmatrix} + \delta \boldsymbol{G}_t^* \begin{bmatrix} u_i^{(1)} \\ v_i^{(1)} \\ w_i^{(1)} \end{bmatrix} + \delta \boldsymbol{G}_\tau^* \begin{bmatrix} u_{i\tau}^{(1)} \\ v_{i\tau}^{(1)} \\ w_{i\tau}^{(1)} \end{bmatrix} \\ &\quad - \tau_* \boldsymbol{G}_\tau^* \frac{\partial}{\partial T_2} \begin{bmatrix} u_{i\tau}^{(1)} \\ v_{i\tau}^{(1)} \\ w_{i\tau}^{(1)} \end{bmatrix} + \tau_* \boldsymbol{N}^{(3)}. \end{aligned} \tag{22}$$

Considering the solution of Eq. (20), we obtain

$$\begin{bmatrix} u_i^{(1)} \\ v_i^{(1)} \\ w_i^{(1)} \end{bmatrix} = \Psi_i(T_2)\boldsymbol{p}\mathrm{e}^{\mathrm{i}\omega_*\tau_* T_0} + \bar{\Psi}_i(T_2)\bar{\boldsymbol{p}}\mathrm{e}^{-\mathrm{i}\omega_*\tau_* T_0}, \tag{23}$$

where $\Psi_i(T_2)$ denotes the complex amplitude, and

$$\boldsymbol{p} = \begin{bmatrix} 1 \\ p_0 \\ p_1 \end{bmatrix} = \begin{bmatrix} 1 \\ \dfrac{a_{21}}{\mathrm{i}\omega_* - a_{22} - K_2} \\ \dfrac{a_{32}}{\mathrm{i}\omega_* - a_{33}} p_0 \end{bmatrix},$$

where $K_2 = [d_2 k_i(1-\mu)]\,\mathrm{e}^{-\mathrm{i}\omega_*\tau_*}$, and correspondingly $K_1 = [d_1 k_i(1-\mu)]\,\mathrm{e}^{-\mathrm{i}\omega_*\tau_*}$.

Then,

$$\begin{aligned}
\left(u_i^{(1)}\right)^2 &= \Psi_i^2(T_2)\,\mathrm{e}^{2\mathrm{i}\omega_*\tau_* T_0} + \bar{\Psi}_i^2(T_2)\,\mathrm{e}^{-2\mathrm{i}\omega_*\tau_* T_0} + 2\left|\Psi_i(T_2)\right|^2,\\
\left(u_i^{(1)}\right)^3 &= \Psi_i^3(T_2)\,\mathrm{e}^{3\mathrm{i}\omega_*\tau_* T_0} + \bar{\Psi}_i^3(T_2)\,\mathrm{e}^{-3\mathrm{i}\omega_*\tau_* T_0}\\
&\quad + 3\Psi_i(T_2)\left|\Psi_i(T_2)\right|^2\mathrm{e}^{\mathrm{i}\omega_*\tau_* T_0}\\
&\quad + 3\bar{\Psi}_i(T_2)\left|\Psi_i(T_2)\right|^2\mathrm{e}^{-\mathrm{i}\omega_*\tau_* T_0}.
\end{aligned}$$

Substituting $\left(u_i^{(1)}\right)^2$, $\left(u_i^{(1)}\right)^3$, and Eq. (23) into Eq. (22), we obtain

$$\begin{aligned}
&\frac{\partial}{\partial T_0}\begin{bmatrix} u_i^{(3)} \\ v_i^{(3)} \\ w_i^{(3)} \end{bmatrix} - \tau_* \boldsymbol{G}_t^* \begin{bmatrix} u_i^{(3)} \\ v_i^{(3)} \\ w_i^{(3)} \end{bmatrix} - \tau_* \boldsymbol{G}_\tau^* \begin{bmatrix} u_{i\tau}^{(3)} \\ v_{i\tau}^{(3)} \\ w_{i\tau}^{(3)} \end{bmatrix}\\
&= \Phi\,\mathrm{e}^{\mathrm{i}\omega_*\tau_* T_0} + \mathrm{NST} + \mathrm{c.c.},
\end{aligned} \tag{24}$$

where NST denotes the non-secular terms, c.c. represents the complex conjugate term, and $\Phi = (\phi^{(1)}, \phi^{(2)}, \phi^{(3)})^{\mathrm{T}}$ with

$$\begin{aligned}
\phi^{(1)} &= -(1+\tau_* K_1)\frac{\partial \Psi_i(T_2)}{\partial T_2} + \delta(a_{11} + a_{13}p_1 + K_1)\Psi_i(T_2)\\
&\quad -3b\tau_*\Psi_i(T_2)\left|\Psi_i(T_2)\right|^2,\\
\phi^{(2)} &= -(1+\tau_* K_2)p_0\frac{\partial \Psi_i(T_2)}{\partial T_2}\\
&\quad +\delta(a_{21} + a_{22}p_0 + p_0 K_2)\Psi_i(T_2),\\
\phi^{(3)} &= -p_1\frac{\partial \Psi_i(T_2)}{\partial T_2} + \delta(a_{32}p_0 + a_{33}p_1)\Psi_i(T_2).
\end{aligned}$$

Equation (24) admits a solution only if the Fredholm solvability condition is satisfied

$$\left\langle \begin{bmatrix} p_2 \\ p_3 \\ p_4 \end{bmatrix}, \begin{bmatrix} \phi^{(1)} \\ \phi^{(2)} \\ \phi^{(3)} \end{bmatrix} \right\rangle = 0, \tag{25}$$

where the inner product is defined by $\langle a, b\rangle = \bar{a}^{\mathrm{T}} b$. To uniquely determine $\bar{p}_2$, $\bar{p}_3$, and $\bar{p}_4$, we impose the normalization condition $\bar{p}_2 + p_0\bar{p}_3 + p_1\bar{p}_4 = 1$. It is straightforward to obtain

$$\begin{aligned}
\bar{p}_2 &= \frac{K_4(a_{33}^2 + \omega_*^2)}{-a_{13}a_{21}a_{32} + (K_3+K_4)(a_{33}^2+\omega_*^2)},\\
\bar{p}_3 &= \frac{K_3K_4(a_{33}^2+\omega_*^2)}{a_{21}(a_{13}a_{21}a_{32} - (K_3+K_4)(a_{33}^2+\omega_*^2))},\\
\bar{p}_4 &= \frac{a_{13}(a_{13} - \mathrm{i}\omega_*)K_4}{a_{13}a_{21}a_{32} - (K_3+K_4)(a_{33}^2+\omega_*^2)},
\end{aligned}$$

where

$$K_3 = a_{11} + \mathrm{i}\omega_* + K_1,\quad K_4 = a_{22} - \mathrm{i}\omega_* + K_2.$$

Using Eq. (25), we obtain

$$\frac{\partial \Psi_i(T_2)}{\partial T_2} = \delta\eta_1\Psi_i(T_2) + \eta_2\Psi_i(T_2)\left|\Psi_i(T_2)\right|^2, \tag{26}$$

where

$$\begin{aligned}
\eta_1 &= \frac{1}{\bar{p}_2(1+\tau_*K_1) + \bar{p}_3 p_0(1+\tau_*K_2) + \bar{p}_4 p_1}\\
&\quad \times\left[\bar{p}_2(a_{11} + a_{13}p_1 + K_1) + \bar{p}_3(a_{21} + a_{22}p_0 + p_0K_2)\right.\\
&\quad \left.+\bar{p}_4(a_{32}p_0 + a_{33}p_1)\right],\\
\eta_2 &= \frac{-3b\tau_*\bar{p}_2}{\bar{p}_2(1+\tau_*K_1) + \bar{p}_3 p_0(1+\tau_*K_2) + \bar{p}_4 p_1}.
\end{aligned}$$

Let $\Psi_i(T_2) = \psi_i\,\mathrm{e}^{-\mathrm{i}\omega_*\tau_* T_2}$, where $\psi_i = \psi_{i1} + \mathrm{i}\psi_{i2}$. Substituting this expression into Eq. (26), we obtain

$$\begin{cases}
\dot{\psi}_{i1} = -\omega_*\tau_*\psi_{i2} + \delta\left(\mathrm{Re}(\eta_1)\psi_{i1} - \mathrm{Im}(\eta_1)\psi_{i2}\right)\\
\qquad\quad + \left(\mathrm{Re}(\eta_2)\psi_{i1} - \mathrm{Im}(\eta_2)\psi_{i2}\right)(\psi_{i1}^2 + \psi_{i2}^2),\\
\dot{\psi}_{i2} = \omega_*\tau_*\psi_{i1} + \delta\left(\mathrm{Re}(\eta_1)\psi_{i2} + \mathrm{Im}(\eta_1)\psi_{i1}\right)\\
\qquad\quad + \left(\mathrm{Re}(\eta_2)\psi_{i2} + \mathrm{Im}(\eta_2)\psi_{i1}\right)(\psi_{i1}^2 + \psi_{i2}^2),
\end{cases} \tag{27}$$

where $\mathrm{Re}(\cdot)$ and $\mathrm{Im}(\cdot)$ denote the real and imaginary parts of the corresponding quantity, respectively.

Finally, letting $\psi_{i1} = \rho_i\cos\theta_i$ and $\psi_{i2} = \rho_i\sin\theta_i$, Eq. (27) becomes

$$\begin{cases}
\dot{\rho}_i = \delta\mathrm{Re}(\eta_1)\rho_i + \mathrm{Re}(\eta_2)\rho_i^3,\\
\dot{\theta}_i = \omega_*\tau_* + \delta\mathrm{Im}(\eta_1) + \mathrm{Im}(\eta_2)\rho_i^2,
\end{cases} \tag{28}$$

where $R_1 = \mathrm{Re}(\eta_1)$ and $R_2 = \mathrm{Re}(\eta_2)$.

Theorem 4

The direction of the Hopf bifurcation is determined by Eq. (28) as follows:

(i) If $R_1R_2 > 0$, system (3) does not undergo a Hopf bifurcation;

(ii) If $R_1R_2 < 0$, a Hopf bifurcation occurs, and its type is characterized as follows:

(*) $R_1 > 0$ (supercritical Hopf bifurcation): the bifurcating periodic solution is stable;

(**) $R_1 < 0$ (subcritical Hopf bifurcation): the bifurcating periodic solution is unstable.

Proof

The amplitude equation (28) possesses a unique positive equilibrium

$$\rho_i = \sqrt{\frac{-\delta R_1}{R_2}},$$

which implies that the existence condition for Hopf bifurcation is $R_1R_2 < 0$, thereby proving (i). Furthermore, Eq. (28) admits the solution

$$\rho_i = \frac{\pm\sqrt{(C\delta R_1\,\mathrm{e}^{-2\delta R_1 T_2} - R_2)\delta R_1}}{C\delta R_1\,\mathrm{e}^{-2\delta R_1 T_2} - R_2},$$

where C is an arbitrary constant. Applying linear stability analysis to the positive equilibrium yields the result in (ii). This completes the proof.

4. Numerical results and discussion

In this section, the stability, the conditions for a Hopf bifurcation, and the role of the BA scale-free network with $N = 100$ nodes in system (3) are investigated. The parameters are set to $a = 0.5$, $b = 1$, $c = -0.9$, $\varepsilon = 0.3$, and $\beta = 1$, resulting in an equilibrium point of $(u_0, v_0, w_0) = (0.928459, 0.028459, 0.028459)$. Crucially, these parameter choices place the intrinsic timescale of the neuronal dynamics within a biologically relevant regime. This enables the model to capture characteristic frequency bands associated with pathological states, laying the groundwork for exploring the Parkinson's disease (PD)-related beta-band oscillations discussed later.

4.1. The stability without time delay

In this section, the Routh–Hurwitz criterion is employed to analyze the case without the time delay τ. Since all terms in conditions H_{11}, H_{12}, H_{13}, and H_{14}, except for σ, are constants, these conditions can be regarded as functions of σ. By analyzing the corresponding curves with σ as the independent variable, the stability of system (3) can be assessed. The results shown in Fig. 1(a) indicate that system (3) is stable, while Fig. 1(b) further confirms this conclusion, thereby providing a basis for the subsequent analysis.

We next investigate whether the selected coupling strengths d_1 and d_2 affect the stability of system (3) in the absence of the time delay τ. Since conditions H_{21}, H_{22}, H_{23}, and H_{24} depend on both σ and the network eigenvalue Λ_α, we further examine the influence of Λ_α for both Laplacian ($\mu = 1$) and quasi-Laplacian ($\mu = 0.5$) networks under fixed σ. The criterion indicates that system (3) remains stable (see Figs. 2 and 3). The red dots on the curves denote the corresponding values of the network eigenvalues. Figures 2 and 3 further verify that the selected parameter set maintains the stability of system (3), thereby providing a foundation for the subsequent investigation of time-delay-induced Hopf bifurcation.

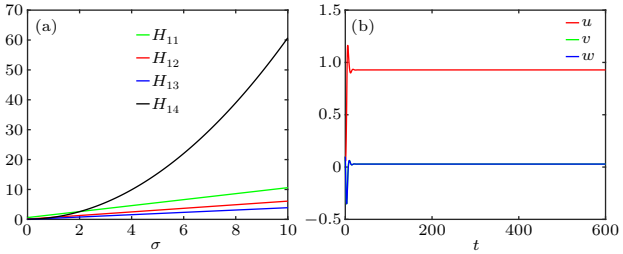


Fig. 1. The Routh–Hurwitz stability criterion is employed to assess the stability of system (3) for the case $d_1 = d_2 = 0$.

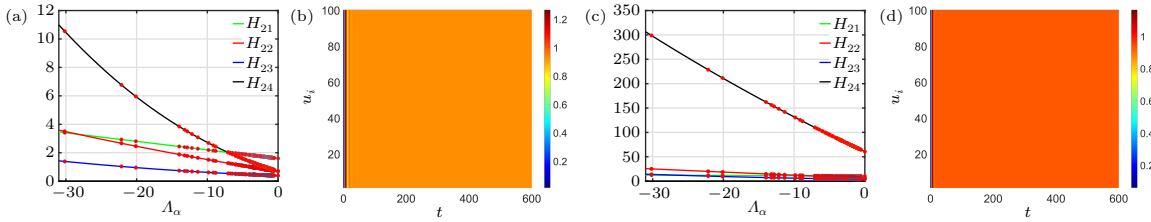


Fig. 2. Routh–Hurwitz stability criterion for assessing the stability of system (3) under $\mu = 1$, $\tau = 0$, $d_1 = 0.05$, and $d_2 = 0.01$. (a) Curves of H_{21}, H_{22}, H_{23}, and H_{24} for $\sigma = 1$. (b) Corresponding spatial patterns. (c) Curves of H_{21}, H_{22}, H_{23}, and H_{24} for $\sigma = 10$. (d) Corresponding spatial patterns.

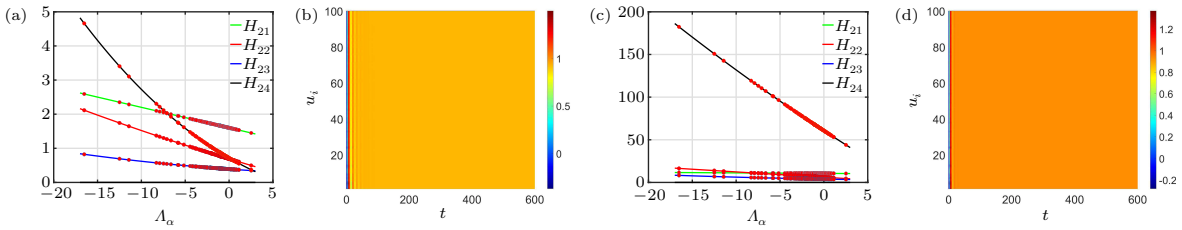


Fig. 3. Routh–Hurwitz stability criterion for assessing the stability of system (3) under $\mu = 0.5$, $\tau = 0$, $d_1 = 0.05$, and $d_2 = 0.01$. (a) Curves of H_{21}, H_{22}, H_{23}, and H_{24} for $\sigma = 1$. (b) Corresponding spatial patterns. (c) Curves of H_{21}, H_{22}, H_{23}, and H_{24} for $\sigma = 10$. (d) Corresponding spatial patterns.

4.2. The stability with time delay τ

In this section, we examine how the time delay τ together with a fixed σ affects neuronal firing. The oscillation frequencies emerging across all unstable delayed regimes (approximately 15–30 Hz) fall strictly within the characteristic beta band, which is closely associated with PD. These results corroborate the relationship between the model and the pathological synchronous rhythms observed in neurological disorders. Finally, we establish the interrelation among the network eigenvalues Λ_α, τ, and σ.

The neuronal firing dynamics in the Laplacian network ($\mu = 1$) were first examined, with the cases of $\sigma = 1$ (Fig. 4) and $\sigma = 10$ analyzed separately. For the Laplacian network with $\sigma = 1$, the critical time delay was calculated as $\tau_* = 1.08665$. When $\tau = 1$, system (3) remains stable (Fig. 4(a)) with an oscillation frequency of 0 Hz; when $\tau = 1.3$, a Hopf bifurcation occurs (Fig. 4(b)), triggering an oscillation fre-

quency of 23.03 Hz; and when $\tau = 2.3$, the amplitude becomes more pronounced (Fig. 4(c)), with the frequency shifting to 23.32 Hz. For $\sigma = 10$ (Appendix B, Fig. B1), the critical time delay was found to be $\tau_* = 1.05239$. Stability is observed at $\tau = 1$, while a Hopf bifurcation occurs at $\tau = 1.3$, generating an oscillation frequency of 24.26 Hz, and becomes significant at $\tau = 2.3$, yielding a frequency of 23.83 Hz.

Subsequently, the neuronal firing dynamics in the quasi-Laplacian network ($\mu = 0.5$) were investigated, again considering $\sigma = 1$ and $\sigma = 10$. For the quasi-Laplacian network with $\sigma = 1$ (Appendix B, Fig. B2), the critical time delay was calculated as $\tau_* = 1.78073$. The system (3) is stable at $\tau = 1.7$ (0 Hz), a Hopf bifurcation occurs at $\tau = 2$ with an oscillation frequency of 15.10 Hz, and the amplitude becomes pronounced at $\tau = 3$, reaching a frequency of 16.08 Hz. For $\sigma = 10$ (Appendix B, Fig. B3), the critical time delay was obtained as $\tau_* = 1.88462$. Stability is maintained at $\tau = 1.8$ (0 Hz), a Hopf bifurcation emerges at $\tau = 2$, oscillating at 16.11 Hz, and it becomes significant at $\tau = 3$, with a frequency of 17.84 Hz.

In all cases, increasing the time delay τ beyond a critical threshold leads to the onset of oscillatory instability, with larger delays resulting in stronger oscillations. For clarity of presentation, the corresponding figures are provided in Appendix B (Figs. B1–B3). Compared with the Laplacian case, the delayed onset of oscillations reflects the reduced effective coupling strength associated with the quasi-Laplacian network. These results indicate that modifying the network coupling structure directly alters the critical conditions for delay-induced Hopf bifurcations. To identify the intrinsic connections and elucidate their biological mechanisms, Fig. 5 is provided.

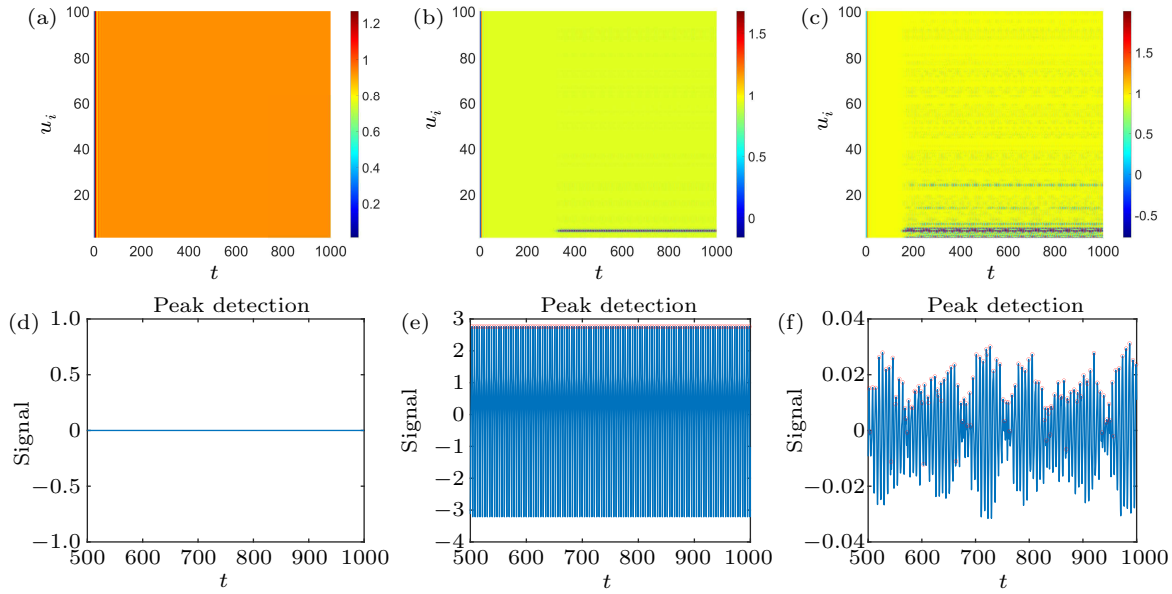


Fig. 4. The stability of system (3) when $\mu = 1$, $\sigma = 1$. (a) The system (3) is stable at $\tau = 1$. (b) Hopf bifurcation occurs at $\tau = 1.3$. (c) The amplitude becomes more pronounced when $\tau = 2.3$. (d)–(f) The oscillation frequencies are 0 Hz, 23.03 Hz, and 23.32 Hz, respectively, indicating the emergence of PD-related dynamics.

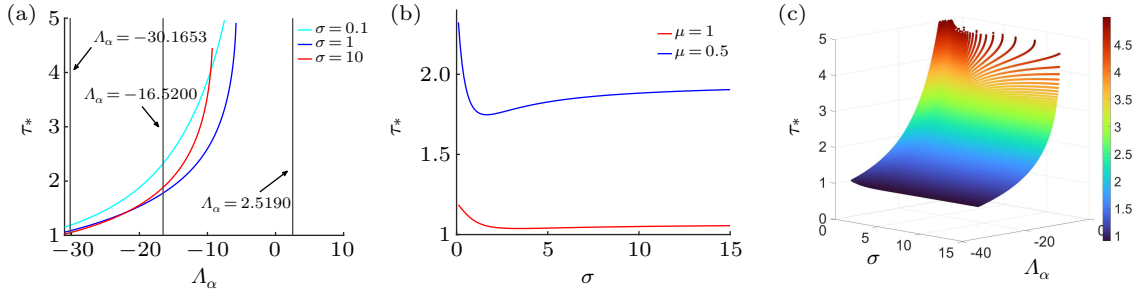


Fig. 5. (a) Relationship between Λ_α and τ_*. (b) Relationship between σ and τ_*. (c) Relationship among Λ_α, σ, and τ_*.

Figure 5 illustrates the relationship among the Laplacian eigenvalue Λ_α, the parameter σ, and the critical time delay τ_*. When Q_{ij} is the Laplacian matrix ($\mu = 1$), the spectral interval is given by $[\Lambda_{\alpha_{\min}}, \Lambda_{\alpha_{\max}}] = [-30.1653, 0]$; for the quasi-Laplacian matrix ($\mu = 0.5$), the interval becomes $[\Lambda_{\alpha_{\min}}, \Lambda_{\alpha_{\max}}] = [-16.5200, 2.5190]$.

As shown in Fig. 5(a), the critical time delay τ_* of system (3) is determined by the smallest negative eigen-

value. Numerical solutions of Eq. (12) indicate that for $\Lambda_\alpha \in [-16.5200, 2.5190]$, either no positive real root exists or the obtained root does not yield the minimal τ. Hence, the admissible range is $\Lambda_\alpha \in [-30.1653, -16.5200]$, which corresponds to τ_* associated with $\mu \in [0.5, 1]$. The values of τ_* displayed in Fig. 5(a) are in full agreement with those computed from Eq. (13). In system (3), the parameter σ characterizes the decay rate of the kernel function associated with the distributed delay, representing the memory length of past inputs for a single neuron. The parameter τ, appearing in the diffusion term, denotes the fixed transmission time delay of coupling signals between different neurons. The emergence of oscillations (Hopf bifurcation) results from the interplay between intrinsic memory effects and the network topology.

In Fig. 5(b), when σ is small, a single neuron averages over a long history of inputs, resulting in sluggish response of its intrinsic dynamics. In this case, a larger τ is required to accumulate sufficient phase shift through network propagation to trigger oscillations. For intermediate values of σ, the memory length of a neuron matches the timescale of the diffusion delay τ, yielding the minimal critical value of τ. Conversely, when σ is large, neurons rely almost entirely on instantaneous inputs, and the distributed delay approximates an instantaneous term. The lack of intrinsic feedback necessitates a larger network delay τ to induce oscillations. From a neuropathological perspective, this optimal matching between neuronal memory and transmission delay provides a mechanistic explanation for the beta-band (15–30 Hz) oscillations highlighted previously. In PD, changes in conduction delays, often stemming from dopamine depletion, can push the network across this minimal critical threshold τ_*, thereby triggering pathological synchronous rhythms.

Overall, these results demonstrate that delay-induced neuronal oscillations are jointly regulated by the network eigenvalues and distributed delay effects, with the smallest negative eigenvalue determining the bifurcation threshold and the parameter σ acting as a dynamical modulator of this threshold.

4.3. Oscillation analysis of network nodes

In Fig. 6, the bifurcations of these nodes are asynchronous: some nodes undergo bifurcation earlier, while others bifurcate later; some exhibit smaller bifurcation amplitudes, whereas others display larger amplitudes. As τ increases, the number of bifurcated nodes grows until all 100 nodes bifurcate. What accounts for this difference? We approach the analysis from the perspective of node degree.

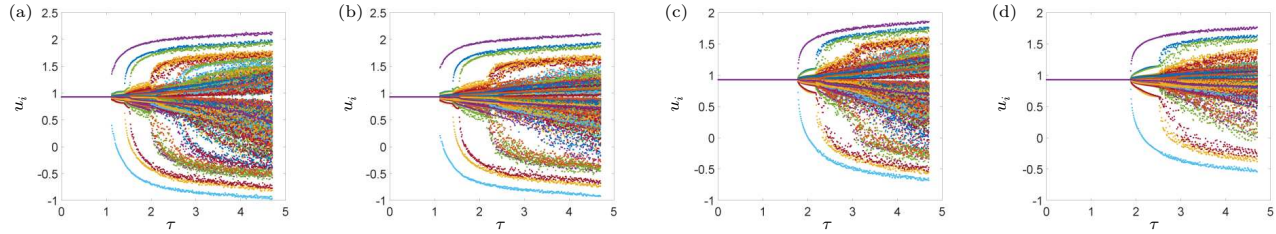


Fig. 6. Hopf bifurcation of u_i in system (3) with respect to τ when $d_1 = 0.05$ and $d_2 = 0.01$. (a) $\mu = 1$, $\sigma = 1$. (b) $\mu = 1$, $\sigma = 10$. (c) $\mu = 0.5$, $\sigma = 1$. (d) $\mu = 0.5$, $\sigma = 10$.

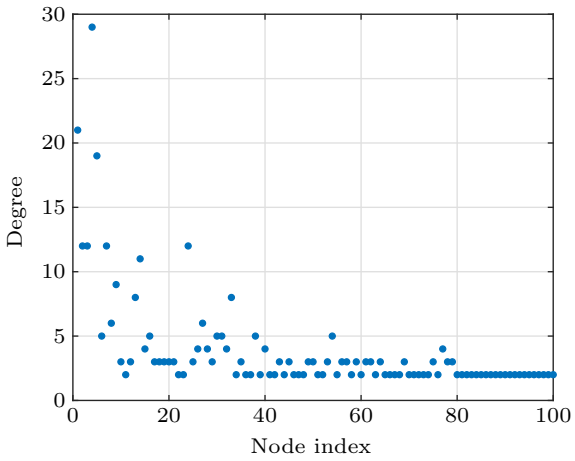


Fig. 7. Degree distribution of the BA scale-free network with 100 nodes.

A BA scale-free network consisting of 100 nodes is considered. Figure 7 displays the degree distribution of the network, where nodes with smaller indices exhibit higher degrees, whereas those with larger indices possess lower degrees.

Hub nodes, by virtue of their high degree, are associated with a coupling network that possesses large negative eigenvalues, leading to an effective amplification of coupling-induced feedback. As a result, hub nodes experience a stronger cumulative influence from the network and reach the Hopf bifurcation threshold at relatively shorter transmission delays τ (Fig. 8). This mechanism explains why hub neurons are preferentially destabilized and become the first sites of oscillation onset in heterogeneous networks. Beyond the early onset of oscillations, the enhanced effective coupling at hub nodes also promotes larger oscillation amplitudes after the bifurcation. Once the steady state loses stability, the collective feedback from multiple connections sustains stronger nonlinear oscillations in hub neurons, manifested as larger membrane potential amplitudes and more pronounced firing activity (Fig. 9). This behavior reflects a network-induced enhancement of neuronal excitability rather than an intrinsic difference in single-neuron dynamics.

In contrast, peripheral nodes possess significantly fewer connections. Their dynamics are primarily shaped by local interactions rather than global network feedback. Peripheral nodes that are topologically close to hubs receive indirect amplification through hub-mediated pathways, allowing them to oscillate with relatively smaller delays and moderate amplitudes. Conversely, peripheral nodes that are weakly connected or distant from hubs experience insufficient cumulative feedback, requiring larger delays to destabilize the steady state and exhibiting smaller oscillation amplitudes.

Consequently, while hub nodes display robust and coherent oscillatory behavior, peripheral nodes exhibit more heterogeneous responses. The distribution of critical delay and oscillation amplitude among peripheral nodes is therefore broader and more uniform, reflecting their weaker and more variable effective coupling within the network. Biologically, this hub-driven amplification closely mirrors the localized hypersynchrony observed in the brains of Parkinson's disease patients. Highly connected regions, such as the subthalamic nucleus (STN), function as structural hubs that are inherently more susceptible to delay-induced instability, thus acting as the primary pacemakers for pathological beta-band tremors.

Next, we aim to establish a connection between the amplitude Eq. (28), derived via the MTS method, and the network topology. For R_1 and R_2 in Eq. (28), when $\mu = 1$, i.e., a Laplacian network, we have $K_1 = K_2 = 0$, and thus R_1 and R_2 do not depend on the node degree k_i. Each of the four subfigures in Fig. 10 contains a single curve, thereby illustrating the bifurcation behavior of the system (3) as a whole. For both $\sigma = 1$ and $\sigma = 10$, when $\Lambda_\alpha = -30.1653$, the conditions $R_1R_2 < 0$ and $R_1 > 0$ are satisfied. According to Theorem 1, a stable Hopf bifurcation occurs, which is consistent with the results in Figs. 6(a) and 6(b).

When $\mu = 0.5$, i.e., a quasi-Laplacian network, R_1 and R_2 incorporate the node degree k_i. Figure 11 displays the variation of R_1 and R_2 with respect to the eigenvalues for nodes of different degrees. For both $\sigma = 1$ and $\sigma = 10$, when $\Lambda_\alpha = -16.5200$, the conditions $R_1R_2 < 0$ and $R_1 > 0$ are satisfied. Hence, by Theorem 1, a stable Hopf bifurcation occurs, in agreement with Figs. 6(c) and 6(d).

The reason why R_1R_2 increases with Λ_α and eventually becomes positive is that the MTS method provides only a local criterion near the bifurcation point and may lose validity away from it. Moreover, the fact that nodes of different degrees bifurcate near $\Lambda_\alpha = -16.5200$ can be explained by Fig. 8, which shows that for each degree there are nodes that bifurcate precisely at the minimum first-oscillation delay τ. In other words, once bifurcation occurs for a node of a given degree, it implies that all nodes with the same degree undergo bifurcation.

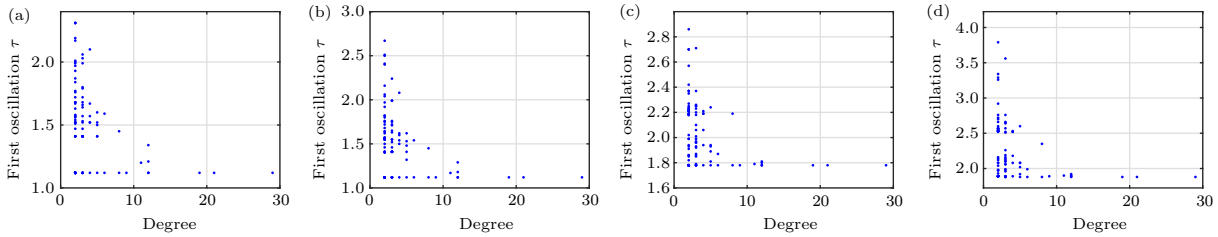


Fig. 8. The distribution of τ for the first oscillation across different degrees. (a) $\mu = 1$, $\sigma = 1$. (b) $\mu = 1$, $\sigma = 10$. (c) $\mu = 0.5$, $\sigma = 1$. (d) $\mu = 0.5$, $\sigma = 10$. In all four subfigures, the onset of the first oscillation exhibits an overall decreasing trend as the node degree increases.

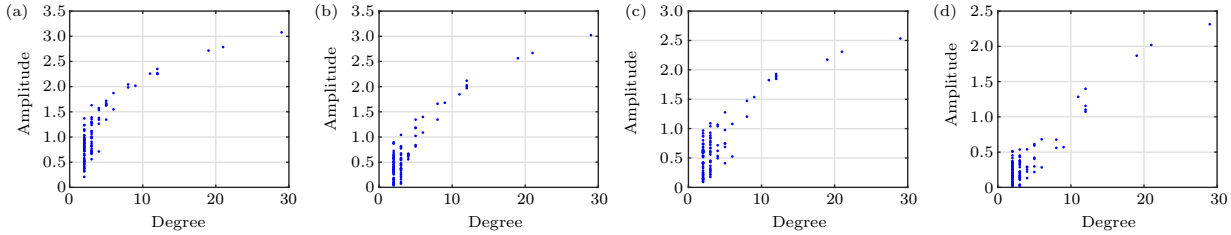


Fig. 9. The distribution of amplitude across different degrees. (a) $\mu = 1$, $\sigma = 1$. (b) $\mu = 1$, $\sigma = 10$. (c) $\mu = 0.5$, $\sigma = 1$. (d) $\mu = 0.5$, $\sigma = 10$. In all four subfigures, the amplitude exhibits an overall increasing trend with increasing node degree.

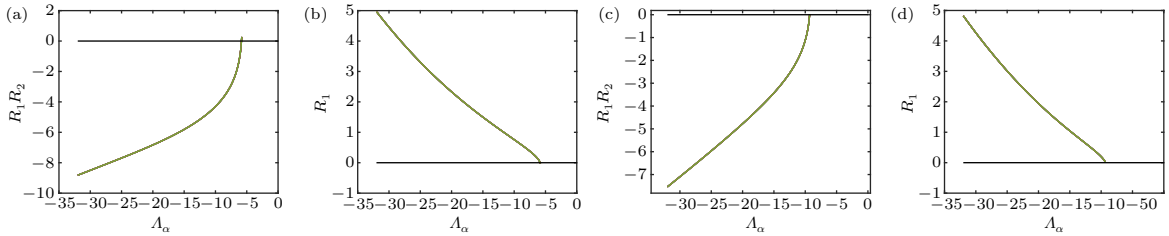


Fig. 10. The distributions of R_1 and R_2 with respect to Λ_α when $\mu = 1$. (a) Distribution of R_1R_2 when $\sigma = 1$. (b) Distribution of R_1 when $\sigma = 1$. (c) Distribution of R_1R_2 when $\sigma = 10$. (d) Distribution of R_1 when $\sigma = 10$.

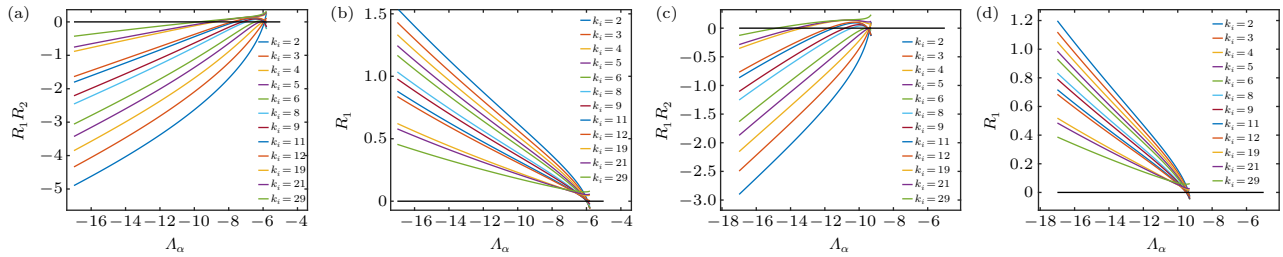


Fig. 11. The distributions of R_1 and R_2 with respect to Λ_α and different node degrees when $\mu = 0.5$. (a) Distribution of R_1R_2 when $\sigma = 1$. (b) Distribution of R_1 when $\sigma = 1$. (c) Distribution of R_1R_2 when $\sigma = 10$. (d) Distribution of R_1 when $\sigma = 10$.

Building on the preceding analysis, we further investigate the statistical relationship between the first-oscillation delay τ, oscillation amplitude, and node degree, aiming to quantify how structural heterogeneity biases delay-induced neuronal dynamics. To this end, 50 independent BA scale-free networks, each consisting of 100 nodes, were generated, and 50 corresponding sets of bifurcation data were collected. Statistical analysis was then employed to extract robust correlations between network topology and oscillatory behavior. Due to the power-law degree distribution of BA networks, the number of nodes decreases rapidly with increasing degree, resulting in limited statistical samples for highly connected hubs. To ensure statistical reliability, we therefore restrict the analysis to degree classes with sufficiently large populations while preserving the essential heterogeneity of the network.

The mean degree $\langle k \rangle$ serves as an important descriptor of the distribution and is given by

$$\langle k \rangle = \int_{k_{\min}}^{\infty} kp(k)\,\mathrm{d}k, \tag{29}$$

where $p(k) = (\gamma-1)k_{\min}^{2}k^{-\gamma}$.

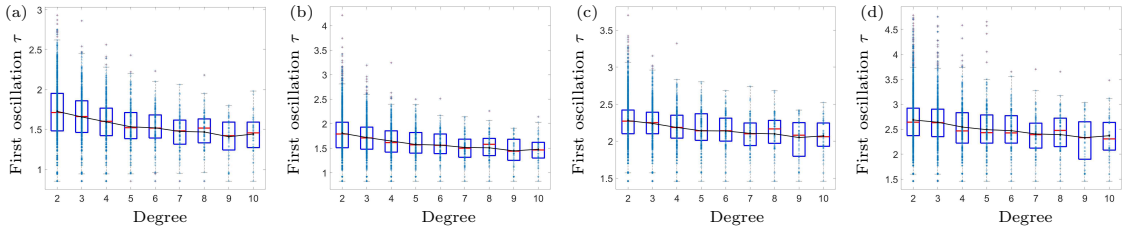


Fig. 12. Box plots and mean values for selected degrees of the first-oscillation delay τ. (a) $\mu = 1$, $\sigma = 1$. (b) $\mu = 1$, $\sigma = 10$. (c) $\mu = 0.5$, $\sigma = 1$. (d) $\mu = 0.5$, $\sigma = 10$.

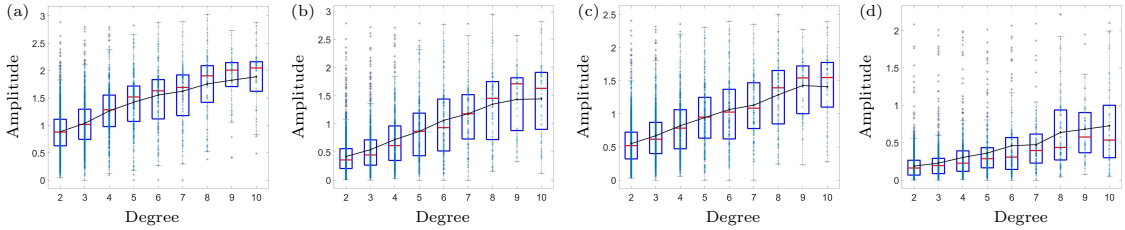


Fig. 13. Box plots and mean values for selected degrees of the oscillation amplitude. (a) $\mu = 1$, $\sigma = 1$. (b) $\mu = 1$, $\sigma = 10$. (c) $\mu = 0.5$, $\sigma = 1$. (d) $\mu = 0.5$, $\sigma = 10$.

In BA networks, γ is generally taken to be 3. With $k_{\min} = 2$ in our generated networks, we obtain $\langle k \rangle = 4$, indicating that most nodes have degrees close to 4. In other words, most nodes are weakly connected and only a small fraction of nodes act as hubs. For the statistical analysis, degrees between 2 and 10 were selected. Figures 12 and 13 show boxplots of the data and the corresponding mean values. The results demonstrate that the node degree is negatively correlated with the first-oscillation delay τ, while it is positively correlated with the amplitude. These statistical trends are fully consistent with the dynamical mechanism identified in Figs. 8 and 9, confirming that highly connected nodes are preferentially destabilized and sustain stronger oscillatory activity due to enhanced effective coupling.

Finally, the means and medians from Figs. 12 and 13 were compared. The results are shown in Fig. 14. Figure 14 demonstrates the overall variation characteristics of neurons and emphasizes the role of degree heterogeneity in shaping collective oscillatory behavior. To quantitatively characterize the correlation among node degree, the first-oscillation delay τ, and amplitude, we calculated Spearman's rank correlation coefficients ρ and the corresponding p-values for statistical significance.

Figures 14(a) and 14(b) show that for both the Laplacian network ($\mu = 1$) and the quasi-Laplacian network ($\mu = 0.5$), when $\sigma \geq 1$, the first-oscillation delay τ of system (3) in-

creases as σ increases. When σ decreases, the first-oscillation delay τ also decreases. Figures 14(a) and 14(b) show that node degree is negatively correlated with the first-oscillation delay τ. Figures 14(c) and 14(d) show that, under the same conditions, the amplitude of system (3) decreases as σ increases. Conversely, the amplitude increases as σ decreases. Figures 14(c) and 14(d) show that node degree is negatively correlated with amplitude. The neuronal response depends not only on the current state but also on the accumulation of past inputs. This behavior reflects the role of the distributed delay parameter σ as a regulator of neuronal memory. As σ increases, the weak kernel decays more rapidly, causing neuronal signals to rely almost entirely on instantaneous input. In the absence of sufficient accumulation, a larger network time delay is required to induce oscillations, and the oscillation amplitude decreases progressively. Conversely, as σ decreases, the weak kernel decays more slowly, enabling neurons to integrate more historical inputs. In this case, even a small network time delay is sufficient to trigger oscillations, and the oscillation amplitude increases accordingly.

Figures 14(a) and 14(b) further show that for both network types, when μ increases, the first-oscillation delay τ decreases, whereas smaller values of μ shift the onset of oscillations to larger delays. Consistently, Figs. 14(c) and 14(d) demonstrate that the oscillation amplitude increases with larger μ and decreases as μ is reduced. Since $Q_{ij} = A_{ij} - \mu k_i \delta_{ij}$, with $\mu \in [0, 1]$, an increase in μ corresponds to stronger self-feedback of the neurons, making them more sensitive to their own activity. In this case, a smaller network time delay is sufficient to induce oscillations, and the oscillation amplitude becomes larger. Conversely, when μ decreases, self-feedback is weakened, and the neurons rely more heavily on the activity of neighboring nodes. In this case, a larger network time delay is required to trigger oscillations, and the oscillation amplitude becomes smaller.

From a neurophysiological perspective, these mathematical dependencies offer insights into the pathogenesis of PD. The distributed delay parameter σ acts as a proxy for the time window of synaptic integration. Clinical evidence suggests that dopamine depletion in PD abnormally alters synaptic integration times in the basal ganglia (effectively corresponding to a smaller σ). As the model demonstrates, this slower decay of historical inputs lowers the delay threshold required to trigger oscillations and amplifies their magnitude. Furthermore, the parameter μ captures the balance between local self-feedback and network-mediated interactions. In the Parkinsonian state, the loss of dopaminergic modulation disrupts local auto-inhibition within core nuclei such as the STN. The findings reveal that such alterations in self-feedback (μ) sensitize the network, providing a mathematical explanation for how localized pathological changes in intrinsic cellular properties can synergize with transmission delays to precipitate the widespread beta-band synchronization characteristic of PD.

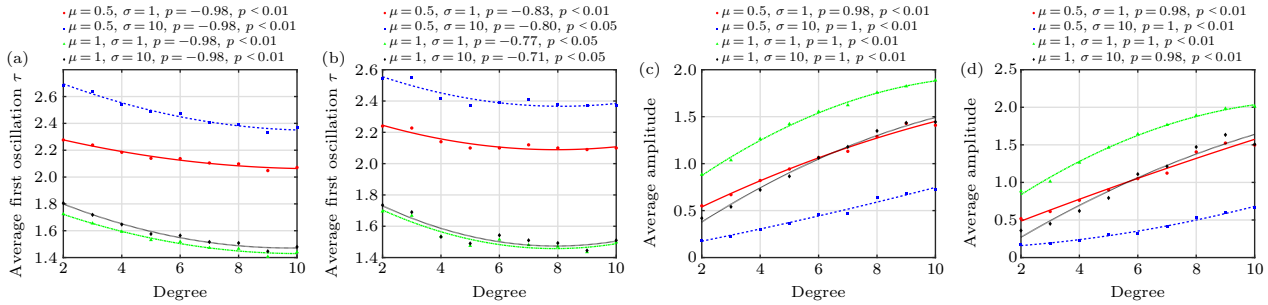


Fig. 14. Multiple-curve comparison figure. (a) Mean value curves of the first-oscillation delay τ, showing a negative correlation between τ and node degree. (b) Median value curves of the first-oscillation delay τ, showing a negative correlation between τ and node degree. (c) Mean value curves of amplitude, showing a positive correlation between amplitude and node degree. (d) Median value curves of amplitude, showing a positive correlation between amplitude and node degree.

5. Conclusion

This study establishes a comprehensive theoretical framework linking network topology, dual time delay effects, and neuronal oscillatory dynamics within a biologically motivated FHN model. By employing the MTS method, we derived reduced amplitude equations that explicitly connect Hopf bifurcation properties to the network structure through the degree distribution k_i, thereby revealing the role of structural heterogeneity in shaping pattern formation in neuronal populations.

The onset of oscillations is governed by a delay-induced Hopf bifurcation, where the critical threshold τ_* is determined by the combined effects of the network Laplacian eigenvalue, the distributed delay parameter σ, and the transmission delay τ. Extending the analysis to the quasi-Laplacian coupling case, we further demonstrate that the coupling parameter μ significantly reshapes the stability landscape by modulating the balance between self-feedback and network-mediated interactions, thereby controlling the system's susceptibility to rhythmic activity.

Statistical analysis over 50 independent BA scale-free networks confirmed that hub nodes act as dynamical amplifiers, characterized by earlier onset of oscillations and larger

oscillation amplitudes. This structural heterogeneity induces a systematic bias in the spatial organization of collective dynamics, leading to a degree-dependent hierarchy in bifurcation behavior.

From a biological perspective, the emergent oscillations fall within the beta-band frequency range (15–30 Hz), which is a hallmark of PD-related neural activity. Our results suggest that highly connected regions, such as the STN, are intrinsically more vulnerable to delay-induced instability due to enhanced effective feedback. The interplay between intrinsic memory effects governed by σ and transmission delays τ provides a mechanistic explanation for the emergence of pathological synchronization, highlighting an optimal timescale matching that facilitates abnormal collective oscillations.

Moreover, the modulation of oscillatory behavior by μ indicates that disruptions in local self-inhibition can synergistically interact with transmission delays, further promoting beta-band synchronization in pathological states. These findings offer a unified explanation for how structural heterogeneity and delay mechanisms jointly shape both the onset and intensity of rhythmic activity in neuronal systems.

In conclusion, this work integrates bifurcation theory, complex network analysis, and computational neuroscience to elucidate how structural heterogeneity governs delay-induced oscillations in neuronal populations. Beyond providing a theoretical explanation for PD-related beta-band synchronization, the results also offer insights into potential strategies for controlling pathological rhythms through modulation of network coupling and delay parameters.

Appendix A

(a) There are the specific expressions for the parameters $m_1, m_2, m_3, m_4, m_5, m_6, m_7, m_8$ and F as defined in Eq. (7)

$$
\begin{aligned}
m_1 &= \sigma + \beta\varepsilon - F,\\
m_2 &= -(d_1 + d_2)\Lambda_\alpha,\\
m_3 &= \beta\varepsilon\sigma - F\sigma - F\beta\varepsilon,\\
m_4 &= (d_2F - d_2\sigma - d_1\sigma - d_1\beta\varepsilon)\Lambda_\alpha,\\
m_5 &= d_1 d_2 \Lambda_\alpha^2,\\
m_6 &= \varepsilon\sigma(1 - F\beta),\\
m_7 &= (d_2F - d_1\beta\varepsilon)\sigma\Lambda_\alpha,\\
m_8 &= d_1 d_2 \sigma \Lambda_\alpha^2,\\
F &= -3bu_0^2 + 2(b + ab)u_0 - ab.
\end{aligned}
$$

(b) The detailed formulations of parameters A_1, A_2, A_3, B_1, B_2 and B_3 in Eq. (10) are provided below:

$$
\begin{aligned}
A_1 &= \omega_\alpha^3 - m_3\omega_\alpha + m_5\omega_\alpha,\\
A_2 &= m_6 + m_8 - m_1\omega_\alpha^2,\\
A_3 &= m_2\omega_\alpha^2 - m_7,\\
B_1 &= \omega_\alpha^3 - m_3\omega_\alpha - m_5\omega_\alpha,\\
B_2 &= m_1\omega_\alpha^2 - m_6 + m_8,\\
B_3 &= m_4\omega_\alpha.
\end{aligned}
$$

(c) The specific expressions for the parameters in Eq. (11) are as follows:

$$
\begin{aligned}
C_5 &= 2m_1^2 - m_2^2 - 4m_3,\\
C_4 &= m_1^4 - m_1^2m_2^2 - 4m_1^2m_3 + 2m_2^2m_3 + 2m_2^2m_5\\
&\quad -4m_1m_6 + 2m_2m_7 + 6m_3^2 - m_4^2 - 2m_5^2,\\
C_3 &= -4m_1^3m_6 + 2m_1^2m_2m_7 + 2m_1^2m_3^2 - m_1^2m_4^2\\
&\quad -2m_1^2m_5^2 + 2m_1m_2^2m_6 - 2m_1m_2^2m_8\\
&\quad +4m_1m_2m_4m_5 - m_2^2m_3^2 - 2m_2^2m_3m_5\\
&\quad -m_2^2m_5^2 + 8m_1m_3m_6 - 4m_2m_3m_7\\
&\quad +4m_2m_4m_8 - 4m_2m_5m_7 - 4m_3^3 + 2m_3m_4^2\\
&\quad +4m_3m_5^2 - 2m_4^2m_5 + 2m_6^2 - m_7^2 - 2m_8^2,\\
C_2 &= 6m_1^2m_6^2 - m_1^2m_7^2 - 2m_1^2m_8^2 - 4m_1m_2m_6m_7\\
&\quad +4m_1m_2m_7m_8 - 4m_1m_3^2m_6\\
&\quad +2m_1m_4^2m_6 + 2m_1m_4^2m_8 - 4m_1m_4m_5m_7\\
&\quad +4m_1m_5^2m_6 - m_2^2m_6^2 + 2m_2^2m_6m_8 - m_2^2m_8^2\\
&\quad +2m_2m_3^2m_7 - 4m_2m_3m_4m_8 + 4m_2m_3m_5m_7\\
&\quad -4m_2m_4m_5m_6 + 2m_2m_5^2m_7 + m_3^4\\
&\quad -m_3^2m_4^2 - 2m_3^2m_5^2 + 2m_3m_4^2m_5 - m_4^2m_5^2\\
&\quad +m_5^4 - 4m_3m_6^2 + 2m_3m_7^2 + 4m_3m_8^2\\
&\quad -4m_4m_7m_8 + 2m_5m_7^2,\\
C_1 &= -4m_1m_6^3 + 2m_1m_6m_7^2 + 4m_1m_6m_8^2\\
&\quad -2m_1m_7^2m_8 + 2m_2m_6^2m_7 - 4m_2m_6m_7m_8\\
&\quad +2m_2m_7m_8^2 + 2m_3^2m_6^2 - m_3^2m_7^2 - 2m_3^2m_8^2\\
&\quad +4m_3m_4m_7m_8 - 2m_3m_5m_7^2 - m_4^2m_6^2\\
&\quad -2m_4^2m_6m_8 - m_4^2m_8^2 + 4m_4m_5m_6m_7\\
&\quad -2m_5^2m_6^2 - m_5^2m_7^2 + 2m_5^2m_8^2,\\
C_0 &= m_6^4 - m_6^2m_7^2 - 2m_6^2m_8^2 + 2m_6m_7^2m_8\\
&\quad -m_7^2m_8^2 + m_8^4.
\end{aligned}
$$

(d) The specific expressions of parameter D_1, D_2, D_3 and D_4 in Eq. (14) are given as follows:

$$
\begin{aligned}
D_1 &= -3\omega^2\cos\theta - 2m_1\omega\sin\theta + m_3\cos\theta - 2\omega m_5\tau\sin\theta\\
&\quad -2m_8\tau\cos\theta + m_5\cos\theta + \omega^2 m_2\tau - m_7\tau + m_4,\\
D_2 &= -3\omega^2\sin\theta + 2m_1\omega\cos\theta + m_3\sin\theta - 2\omega m_5\tau\cos\theta\\
&\quad +2m_8\tau\sin\theta - m_5\sin\theta + 2m_2\omega - m_4\tau\omega,\\
D_3 &= -m_4\omega^2 - 2m_5\omega^2\cos\theta + 2m_8\omega\sin\theta,\\
D_4 &= -m_2\omega^3 + m_7\omega + 2m_5\omega^2\sin\theta + 2m_8\omega\cos\theta.
\end{aligned}
$$

Appendix B

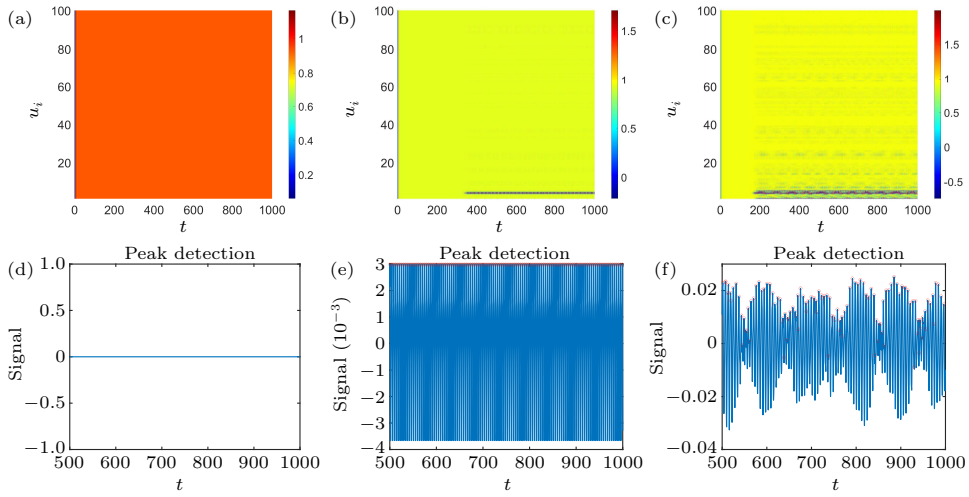


Fig. B1. Stability of system (3) when $\mu = 1$, $\sigma = 10$. (a) The system (3) is stable at $\tau = 1$. (b) Hopf bifurcation occurs at $\tau = 1.3$. (c) The amplitude becomes more pronounced when $\tau = 2.3$. (d)–(f) The oscillation frequencies are 0 Hz, 24.26 Hz, and 23.83 Hz, respectively, indicating the emergence of PD-related oscillations.

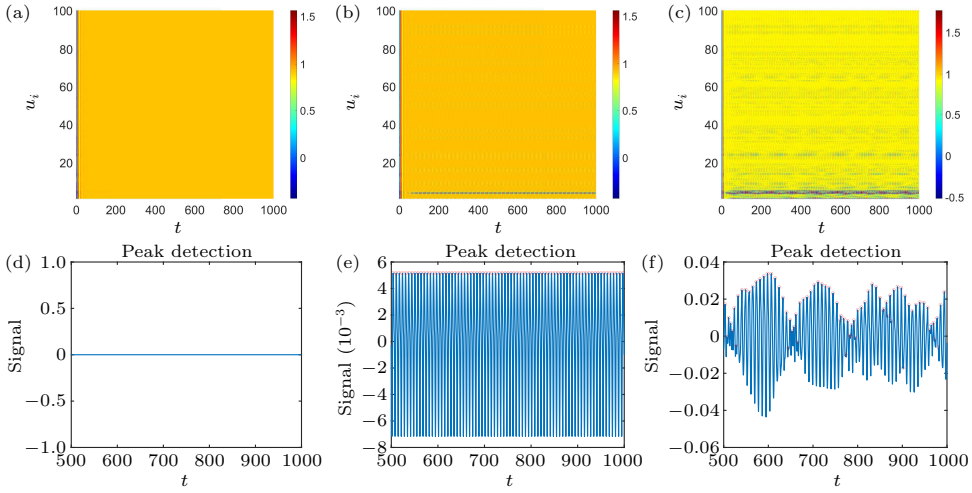


Fig. B2. Stability analysis of system (3) for $\mu = 0.5$, $\sigma = 1$. (a) The system is stable at $\tau = 1.7$. (b) Hopf bifurcation occurs at $\tau = 2$. (c) The oscillation amplitude becomes more pronounced at $\tau = 3$. (d)–(f) The corresponding oscillation frequencies are 0 Hz, 15.10 Hz, and 16.08 Hz, respectively, indicating the emergence of Parkinsonian dynamics.

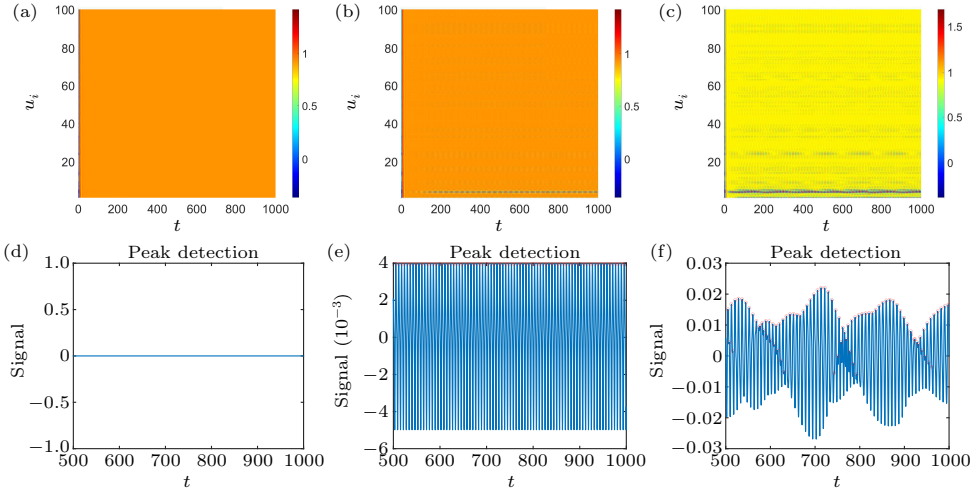


Fig. B3. Stability analysis of system (3) for $\mu = 0.5$, $\sigma = 10$. (a) The system is stable at $\tau = 1.8$. (b) Hopf bifurcation occurs at $\tau = 2$. (c) The oscillation amplitude becomes more pronounced at $\tau = 3$. (d)–(f) The corresponding oscillation frequencies are 0 Hz, 16.11 Hz, and 17.84 Hz, respectively, indicating the emergence of Parkinsonian dynamics.

Acknowledgments

This work was supported by the National Natural Science Foundation of China (Grant Nos. 12272135 and 11971416), the Natural Science Foundation of Henan Province (Grant No. 242300420661), the Training Program for Young Key Teachers in Colleges and Universities of Henan Province (Grant No. 2023GGJS144), the Funding Program of Henan Province for Merit-based Overseas Students (Grant No. 2023), and the Postgraduate Education Reform and Quality Improvement Project of Henan Province (Grant No. YJS2026AL002).

References

[1] Hodgkin A L and Huxley A F 1952 *J. Physiol.* **117** 500
[2] FitzHugh R 1961 *Biophys. J.* **1** 445
[3] Aram Z, Jafari S, Ma J, Sprott J C, Zendehrouh S and Pham V T 2017 *Commun. Nonlinear Sci. Numer. Simul.* **44** 449
[4] Barabási A L and Albert R 1999 *Science* **286** 5439 509
[5] Tanaka G, Morino K and Aihara K 2012 *Sci. Rep.* **2** 232
[6] Moon J Y, Lee U, Blain-Moraes S and Mashour G A 2015 *PLoS Comput. Biol.* **11** e1004225
[7] Kocsis Z, Jenison R L, Taylor P N, Calmus R M, McMurray B, Rhone A E, Sarrett M E, Deifelt C S, Kikuchi Y, Gander P E, Berger J I, Kovach C K, Choi I, Greenlee J D, Kawasaki H, Cope T E, Griffiths T D, Howard M A III and Petkov C I 2023 *Nat. Commun.* **14** 6264
[8] Restrepo J G, Ott E and Hunt B R 2005 *Phys. Rev. E* **71** 036151
[9] Goltsev A V, Dorogovtsev S N, Oliveira J G and Mendes J F F 2012 *Phys. Rev. Lett.* **109** 128702
[10] Turing A M 1952 *Philos. Trans. R. Soc. Lond. B* **237** 37
[11] Nakao H and Mikhailov A S 2010 *Nat. Phys.* **6** 544
[12] Asllani M, Challenger J D, Pavone F S, Sacconi L and Fanelli D 2014 *Nat. Commun.* **5** 4517
[13] Zheng Q Q, Shen J W and Xu Y 2020 *Phys. Rev. E* **102** 062215
[14] Gong R, Wegscheider M, Mühlberg C, Gast R, Fricke C, Rumpf J J, Nikulin V V, Knösche T R and Classen J 2021 *Brain* **144** 487
[15] Guerra A, Colella D, Giangrosso M, Cannavacciuolo A, Paparella G, Fabbrini G, Suppa A, Berardelli A and Bologna M 2022 *Brain* **145** 224
[16] Mathiopoulou V, Lofredi R, Feldmann L K, Habets J, Darcy N, Neumann W J, Faust K, Schneider G H and Kühn A A 2024 *npj Parkinsons Dis.* **10** 77
[17] Pecora L M and Carroll T L 1998 *Phys. Rev. Lett.* **80** 2109
[18] Jia R W 2017 *Fuzzy Sets Syst.* **319** 70
[19] Ji Y S and Mao X C 2024 *Nonlinear Dyn.* **112** 7571
[20] Chen M X and Zheng Q Q 2022 *Chaos Solitons Fractals* **161** 112332
[21] Chen M X, Wu R C, Liu B and Chen L P 2023 *ZAMM* e201900111
[22] Zhang T H and Zang H 2014 *Phys. Rev. E* **90** 052908
[23] Karmeshu, Gupta V and Kadambari K V 2011 *Biol. Cybern.* **104** 369
[24] Anchisi D, Scelfo B and Tempia F 2001 *J. Neurophysiol.* **85** 323
[25] Tiganj Z, Hasselmo M E and Howard M W 2015 *Hippocampus* **25** 27
[26] Atay F M 2003 *Phys. Rev. Lett.* **91** 094101
[27] Atay F M and Hutt A 2005 *SIAM J. Appl. Math.* **65** 644
[28] Jirsa V K and Ding M Z 2004 *Phys. Rev. Lett.* **93** 070602
[29] Petkoski S and Jirsa V K 2019 *Philos. Trans. R. Soc. A* **377** 20180132
[30] Li T Y and Wang Q R 2022 *Int. J. Bifurcation Chaos* **32** 2250133
[31] Xu C J, Zhang Q M and Wu Y S 2016 *Cogn. Comput.* **8** 1103
[32] Zheng Q Q, Shen J W, Pandey V, Guan L N and Guo Y T 2023 *Chaos Solitons Fractals* **168** 113205
[33] Wang Z, Li L, Li Y X and Cheng Z S 2018 *Neural Process Lett.* **48** 1